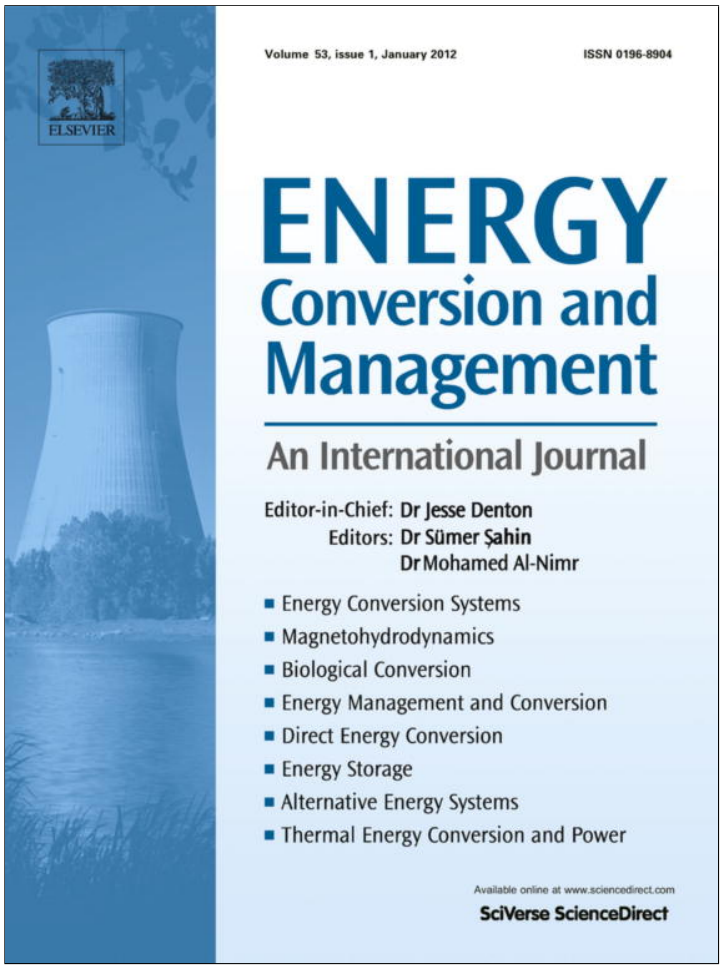

Energy Conversion and Management 74 (2013) 1–8

Contents lists available at SciVerse ScienceDirect

Energy Conversion and Management

journal homepage: www.elsevier.com/locate/enconman

Rotor demagnetization effects on permanent magnet synchronous machines

Cristian Ruschetti [a], Carlos Verucchi [b], Guillermo Bossio [a,*], Cristian De Angelo [a], Guillermo García [a]

[a] Grupo de Electrónica Aplicada, Fac. de Ingeniería, Universidad Nacional de Río Cuarto, Ruta Nac. #36 Km 601, (X5804BYA), Río Cuarto, Córdoba, Argentina
[b] Grupo INTELYMEC, Universidad Nacional del Centro de la Provincia de Buenos Aires, Olavarría, Buenos Aires, Argentina

ARTICLE INFO

Article history:
Received 28 November 2012
Accepted 5 May 2013

Keywords:
Permanent magnet synchronous machine
Demagnetization
Fault detection
Parallel windings
Finite element method

ABSTRACT

The effects of asymmetrical magnet faults on the rotor of Permanent Magnet Synchronous Machines (PMSM) are analyzed in the present work. Two different stator winding configurations, series and parallel connected windings, are considered in the analysis. From PMSM with parallel windings, a fault detection strategy based on the information contained in the branch-current spectrum is proposed. A fault severity factor is defined to quantify demagnetization on a single magnet. This factor is practically independent from the motor load conditions. Simulation results using a finite element model are obtained to evaluate the feasibility of the proposal. Additionally, voltage reduction and current derating due to rotor demagnetization are also evaluated. Experimental results are presented to validate the proposal.

1. Introduction

Permanent Magnet Synchronous Machines (PMSM) are widely used as both motors in industrial drives and generators in renewable energy power plants. In both cases, faults are responsible for high costs due to maintenance and downtime. Recently, fault detection in PMSM has become more noticeable due to the impulse given to the development of renewable energy sources and the increasing tendency to use these machines as generators directly coupled to wind turbines [1,2]. There exist several proposals for monitoring wind turbines, as for instance fault detection in electric generators [3], which mainly aims to reduce maintenance costs.

Faults in PMSM can be classified as: stator faults, rotor faults and bearings faults. For the particular case of PMSM connected to an inverter, faults in either the switches or sensors may also appear.

Rotor faults are commonly due to eccentricity, damage in any of the magnets, asymmetries as well as mechanical looseness [4]. Rotor eccentricity is mainly due to non-uniform distribution of the air-gap and it can be static, dynamic or mixed [5,6]. Eccentricity produces unbalanced radial forces, which can cause stator to rotor rub. For static eccentricity, the position of the minimum air-gap is fixed respect to the stator. On the contrary, for dynamic eccentricity, the rotor center does not coincide with the rotation center and therefore the position of the minimum air-gap rotates with the rotor [7]. Eccentricities may be due to load unbalances, looseness, misalignment, wrong assembly and even bending of the rotor [8].

The presence of faults on the rotor magnets may produce on the PMSM similar effects to those due to dynamic eccentricity. Microscopic fissures, chips, disintegration due to corrosion and even partial demagnetization are some of these magnet faults [9–11].

The Motor Current Signature Analysis (MCSA) technique has been widely used in the detection of induction motor faults such as broken bars and air-gap eccentricity [12–16] and synchronous motor faults such as air-gap eccentricity [17]. In PMSMs, this technique was used for detecting winding faults and dynamic eccentricity [18–20].

As it was presented in literature [4,20–24], rotor faults produces new components on the stator current frequency spectra according to $f_{dm} = f_s\left(1 \pm \frac{k}{P}\right)$ with $k = 1, 2, 3\ldots$, where P is the number of pole pairs and f_s is the stator frequency.

Numerical simulation using the Finite Element Method (FEM) is a very effective tool for the analysis of PMSM faults [25,21]. This method allows a precise evaluation of fault diagnosis strategies for different machine configurations.

Dynamic and static eccentricities as well as demagnetization effects on a single magnet are analyzed in [9] using FEM. This proposal consists in carrying out several static calculations. These calculations include evaluating n steps in order to produce a 360° mechanical rotation of the machine. The air-gap flux waveform is

* Corresponding author. Tel.: +54 358 4676598; fax: +54 358 4676255.
E-mail addresses: cruschetti@ing.unrc.edu.ar (C. Ruschetti), verucchi@fio.unicen.edu.ar (C. Verucchi), gbossio@ing.unrc.edu.ar (G. Bossio), cdeangelo@ing.unrc.edu.ar (C. De Angelo), g.garcia@ing.unrc.edu.ar (G. García).

0196-8904/$ - see front matter © 2013 Elsevier Ltd. All rights reserved.
http://dx.doi.org/10.1016/j.enconman.2013.05.001

then generated from the FEM results. Once the air-gap magnetic field distribution is obtained from the equations that describe the PMSM, the fault analysis is carried out.

Other authors use FEM to evaluate air-gap eccentricity in PMSMs [26]. Simulation results are experimentally validated measuring vibrations using an accelerometer. This is a good alternative to the analysis of the current frequency spectrum.

In [21] an online strategy to detect incipient rotor demagnetization faults in surface-mounted PMSMs with serial windings connection was proposed. Such strategy uses the zero-sequence voltage component instead of the current signature and it is applicable to inverter-fed PMSMs.

A spectral analysis is carried out using time–frequency methods for the detection of rotor faults in brushless DC motors (BLDCM) under non-stationary operation conditions in [4]. In this case, two methods using windowed Fourier ridges and Wigner–Ville-based distributions are used for the detection of the rotor faults frequencies. The analysis is carried out on a six-pole BLDCM and the components used to determine the presence of faults are sidebands at $\frac{2}{3}f_s$ and $\frac{4}{3}f_s$.

The effects of uniform and local demagnetization on PMSMs back-EMF with different winding distribution using a 2-D FEM are analyzed in [24]. The effects of rotor eccentricity on currents and back-EMF of a PM brushless motor with parallel winding connections are also analyzed using FEM in [27].

In this paper, the effects of single magnet demagnetization on the EMF, phase and branch currents are analyzed. This analysis is validated through simulation results using a FEM model of the machine, and experimental results. The FEM model of PMSMs with single magnet demagnetization and different stator winding configurations is simulated using a Finite Element Analysis (FEA) software that allows the calculation of structures with rotation, while avoiding magneto-static calculations. Simulation results are validated through experimental tests on a PMSM prototype. From this analysis, a suitable fault severity factor is proposed.

This paper is structured as follows: An analytical approach for the rotor fault analysis and a proposal for asymmetrical demagnetization detection are presented in Section 2. In Section 3, FEM models for PMSM with serial and parallel connection of windings are obtained. Simulation results using the FEM models are shown in Section 4. Section 5 shows experimental results to validate the proposal and evaluate the current derating due to rotor demagnetization. Finally, discussions and conclusions are given in Section 6.

2. Rotor fault analysis

In order to evaluate the effects of asymmetrical demagnetization, we propose to analyze first the changes caused by this fault on the EMF components. From this analysis, the effects on the currents at each winding are determined and the components to be used for the diagnosis, proposed.

The EMF induced in any stator winding, $e(t)$, can be obtained from the derivative of the linked-flux ψ_s as,

$$e(t) = -\frac{d\psi_s}{dt} = -\frac{d\psi_s}{d\theta_r}\frac{d\theta_r}{dt} = \varphi(\theta_r)\omega_r \tag{1}$$

where θ_r and ω_r are the angular rotor position and speed, respectively.

The flux linked by a stator circuit is obtained by integrating the flux density B on the surface covered by the winding. Assuming radial flux density and uniformity of the windings along the axial axis of the machine, the flux linked by a stator winding is given by,

$$\psi_s(\theta_r) = rl\int_0^{2\pi} N(\theta_s)B(\theta_s - \theta_r)d\theta_s \tag{2}$$

where r is the mean radius of the air gap, l is the axial length and N is the stator winding distribution as a function of a reference angle θ_s in the stator.

In this equation N and B are, in any case, periodic functions over the interval $[0,2\pi]$ and both can be written as Fourier series:

$$N(\theta_s) = \sum_{n=1}^{\infty} N_n \cos(n\theta_s) \tag{3}$$

$$B(\theta_s, \theta_r) = \sum_{m=1}^{\infty} B_m \cos(m(\theta_s - \theta_r)) \tag{4}$$

Then, by replacing (3) and (4) into (2) it yields an integral of a sum of products of sines and cosines. In this integral, the only terms not null are those corresponding to the same frequency ($m = n$), resulting in,

$$\psi_s(\theta_r) = \pi rl\sum_{n=1}^{\infty} N_n B_n \cos(n\theta_r) \tag{5}$$

Then, the EMF is obtained as the time derivative of the linked-flux (5). Considering that the rotor speed is constant, $\theta_r = \omega_r t$ and the EMF is given by,

$$e(t) = K\omega_s\sum_{n=1}^{\infty} nN_nB_n \sin\left(\frac{n\omega_s}{P}t\right) \tag{6}$$

where $K = \frac{\pi rl}{P}$ and $\omega_s = P\omega_r$. From this expression it can be seen that a specific component will appear on the induced EMF only if such component exist in both the windings distribution and the rotor flux distribution. In the case where either N_n or B_n is zero, the corresponding component will not appear in the EMF of the PMSM.

2.1. PMSM with serial connection of windings

For a PMSM with symmetrical windings and P pairs of poles, the winding distribution of a phase is given by

$$N_s(\theta_s) = \sum_{\substack{n=1 \\ n\text{odd}}}^{\infty} N_n \cos(nP\theta_s) \tag{7}$$

As an example, a series winding for a machine with two pairs of poles is shown in Fig. 1.

Moreover, if the rotor is healthy, the flux density can be written as:

$$B(\theta_s, \theta_r) = \sum_{\substack{n=1 \\ n\text{odd}}}^{\infty} B_n \cos(nP(\theta_s - \theta_r)) \tag{8}$$

Repeating the previous steps, the EMF can be expressed as

$$e(t) = K\omega_s\sum_{\substack{n=1 \\ n\text{odd}}}^{\infty} nN_nB_n \sin(n\omega_s t) \tag{9}$$

From (9) it can be observed that only the fundamental frequency $f_s = \frac{\omega_s}{2\pi}$ and its harmonics $f_{sn} = nf_s$ appear in the EMF.

Then, considering asymmetric rotor demagnetization, the flux is asymmetric between each pair of poles and is periodic only within $[0,2\pi]$. For such reason, it can be written as,

$$B_f(\theta_s, \theta_r) = \sum_{m=1}^{\infty} B_m^f \cos(m(\theta_s - \theta_r)) \tag{10}$$

In this equation, when $m = nP$ with $n = 1, 2, 3,\ldots$, we obtain the components of the original flux whose amplitude is reduced by demagnetization. Furthermore, new components appear when $m \neq nP$ due to asymmetric demagnetization and their amplitude depends on the fault severity.

Using (8) and (10) the EMF results in,

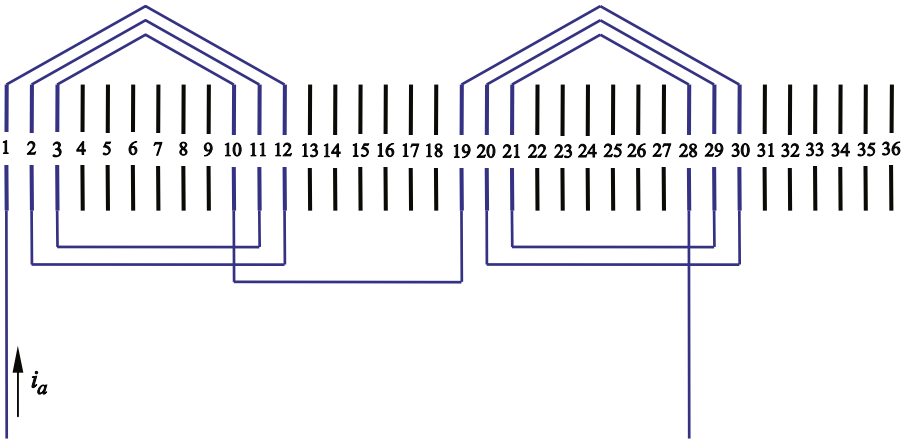

Fig. 1. Serial connection of windings (Phase *a*).

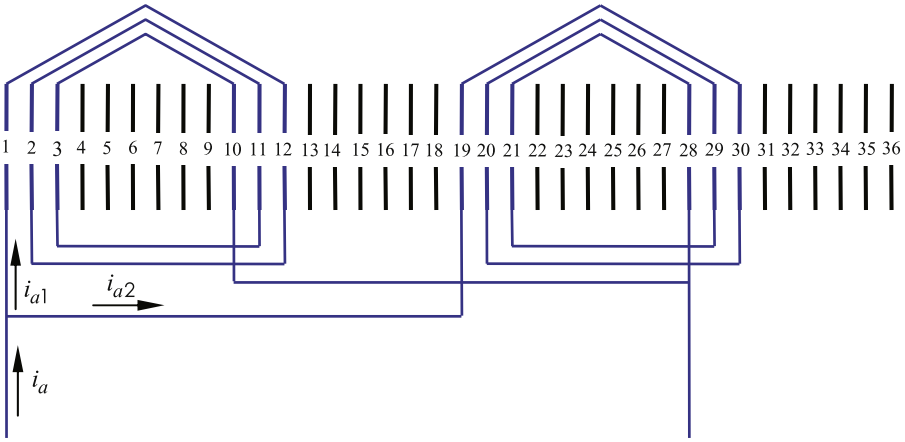

Fig. 2. Parallel connection of windings (Phase *a*).

$$e(t) = K\omega_s \sum_{\substack{n=1 \\ n\text{odd}}}^{\infty} nN_n B_{nP}^f \sin(n\omega_s t) \tag{11}$$

From this equation, it can be seen that for fault in the magnets, a change in the flux distribution changes the amplitude of harmonics in the induced EMF, but it will not produce new components on it. As in the EMF, no new components appear on the stator currents or the electromagnetic torque due to fault. A similar result is obtained with other approach for PMSM with serial connection of windings in [21].

2.2. PMSM with parallel connection of windings

The effects of asymmetric demagnetization on PMSM with parallel windings are analyzed below. To simplify the analysis, only two parallel circuits for a machine with *P* pairs of poles are considered. Besides, an even number of pair of poles is considered so that the parallel circuits are symmetric. As an example, a stator phase with two pair of poles in parallel is shown in Fig. 2. The equivalent circuit for each phase is shown in Fig. 3a.

Under these considerations, it can be demonstrated that the distribution for one of the stator circuits is periodic in the $[0,2\pi]$ interval and it is given by,

$$N_{s1}(\theta_s) = \sum_{\substack{n=1 \\ n\text{odd}}}^{\infty} (N_n^1 \cos(nP\theta_s) + H_n^1 \cos(n\theta_s)) \tag{12}$$

The winding distribution for the other circuit can be obtained by shifting the previous distribution,

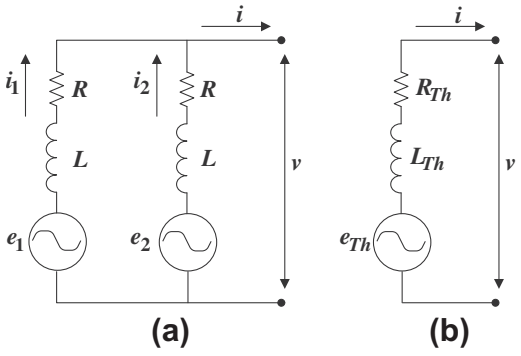

Fig. 3. Equivalent circuits for a stator phase. Parallel circuits (a), Series circuit or Thevenin equivalent circuit.

$$N_{s2}(\theta_s) = N_{s1}(\theta_s + \pi) \tag{13}$$

Thus, the windings distribution for the second circuit can be written as,

$$N_{s2}(\theta_s) = \sum_{\substack{n=1 \\ n\text{odd}}}^{\infty} (N_n^1 \cos(nP\theta_s) - H_n^1 \cos(n\theta_s)) \tag{14}$$

From these equations, it can be seen that by adding these winding distributions to form a series winding, all odd terms are cancelled, resulting in the equation of the serial winding distribution previously obtained in (7), with $N_n = 2N_n^1$.

Furthermore, proceeding in the same way as for the serial case, the EMF on each circuit is,

$$e_1(t) = K\omega_s \sum_{\substack{n=1 \\ n\text{odd}}}^{\infty} \left(nN_n^1 B_{nP}^f \sin(n\omega_s t) + nH_n^1 B_n^f \sin\left(\frac{n\omega_s}{P} t\right)\right) \tag{15}$$

$$e_2(t) = K\omega_s \sum_{\substack{n=1 \\ n\text{odd}}}^{\infty} \left(nN_n^1 B_{nP}^f \sin(n\omega_s t) - nH_n^1 B_n^f \sin\left(\frac{n\omega_s}{P} t\right)\right) \tag{16}$$

As in the case with series windings, the amplitude of harmonics on the EMF at each branch is reduced due to demagnetization. However, unlike the PMSM with serial windings, new components appear in the EMF at the frequencies given by $\frac{nf_s}{P}$ (n odd). These components are in counter-phase into each branch, so that if the two circuits are connected in series, those components are cancelled, obtaining the same result as in (11).

For PMSM with parallel windings, these new components in the EMF do not produce new components in the phase voltage. Indeed, if the Thevenin equivalent circuit is obtained (Fig. 3b), the resulting EMF is given by,

$$e_{Th}(t) = K\omega_s \sum_{\substack{n=1 \\ n\text{odd}}}^{\infty} nN_n^1 B_{nP}^f \sin(n\omega_s t) \tag{17}$$

where it can be seen that the EMF will contain the fundamental component and their harmonics.

However, in each branch, new components at frequency $\frac{nf_s}{P}$ are generated in the branch current, and their magnitude magnitudes are limited by the impedance of the stator circuits. For the case of linear loads, the current in each branch is given by,

$$i_1(t) = \sum_{\substack{n=1 \\ n\text{odd}}}^{\infty} \left(I_n \sin(n\omega_s t + \varphi_n) + I_{n/P} \sin\left(\frac{n\omega_s}{P} t + \varphi_{n/p}\right)\right) \tag{18}$$

$$i_2(t) = \sum_{\substack{n=1 \\ n\text{odd}}}^{\infty} \left(I_n \sin(n\omega_s t + \varphi_n) - I_{n/P} \sin\left(\frac{n\omega_s}{P} t + \varphi_{n/p}\right)\right) \tag{19}$$

And the phase current results in,

$$i(t) = \sum_{\substack{n=1 \\ n\text{odd}}}^{\infty} (2I_n \sin(n\omega_s t + \varphi_n)) \tag{20}$$

Because no new components appear in either the equivalent EMF or the phase currents due to demagnetization, no new components will appear in either the power or torque of the machine.

2.3. Fault detection and severity factor

According to what was developed in the previous section, it is possible to detect asymmetric demagnetization problems through the components that appear in the current branch at frequency $\frac{nf_s}{P}$ (n odd). For PMSMs with two pairs of poles, the most significant components are at $n = 1$ and $n = 3$. The amplitude of those components, at frequencies $\frac{1}{2}f_s$ and $\frac{3}{2}f_s$, are defined as $I_{1/2}$ and $I_{3/2}$, respectively.

We define the fault severity μ, as the percentage of demagnetization in a pole. Therefore, $\mu = 0\%$ corresponds to a healthy rotor and $\mu = 100\%$ to a pole completely demagnetized.

To estimate the severity of the fault, it is necessary to define a severity factor $\hat{\mu}$ based on the characteristic components due to the fault. This severity factor must be insensitive to variations in the operating condition of the PMSM. In a previous work [28] the component $I_{1/2}$ was proposed to define the severity factor. This factor is not very sensitive to the load conditions and shows a good approximation to the percentage of demagnetization in the pole piece. However, this factor requires for its calculation the knowledge of the active power, thus increasing the number of sensors required for the strategy implementation.

For this reason, a new severity factor $\hat{\mu}$, based on the sum of the sideband components is proposed in this work,

$$\hat{\mu} = \left(\frac{I_{1/2} + I_{3/2}}{I_N}\right) 100[\%] \tag{21}$$

where I_N is the peak value of the nominal phase current. To calculate this severity factor only the measurement of a current branch is necessary, so it significantly reduces the number of sensors with respect to the previous proposal.

3. Finite element model of a PMSM

A PM Synchronous generator was used for the simulation and experimental analysis. Fig. 4 shows a simplified scheme of this machine and Table 1 shows the rated data.

Simulation was carried out using a FEM software that allows the calculation of structures with rotation. The characteristics of the materials used in the FEM model were obtained from manufacturer tables. However, the characteristic of electrical steel was provided by GRUCAD laboratory of UFSC [29].

The mesh was chosen based on the calculation precision and with a non-uniform triangular distribution. The air-gap is the section with most element density, because this section presents the highest magnetic field variations, and it is the transition area between rotor and stator during rotation. The final mesh has about 40,000 1st-order triangular elements (Fig. 5). However, the software incorporates, before simulation under rotation, 2nd-order triangular elements with the objective of improving transition between the different calculus positions.

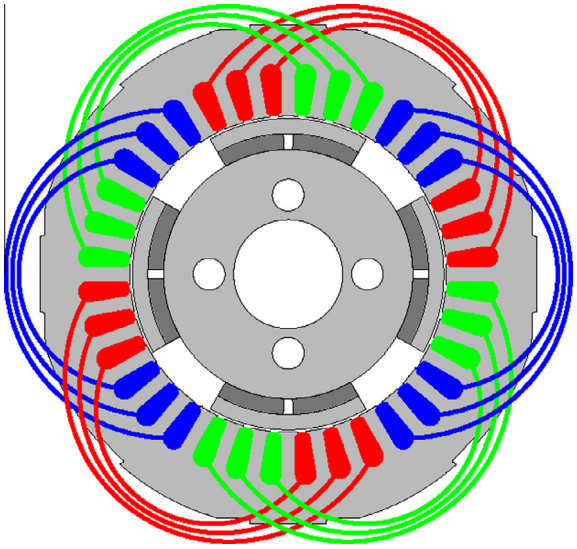

Fig. 4. Simplified scheme of the PM synchronous generator.

Table 1
PMSM rated data.

Pn (kW)	3.0
Vn (V)	200
In (A)	5.0
f (Hz)	50
Pair of poles	2

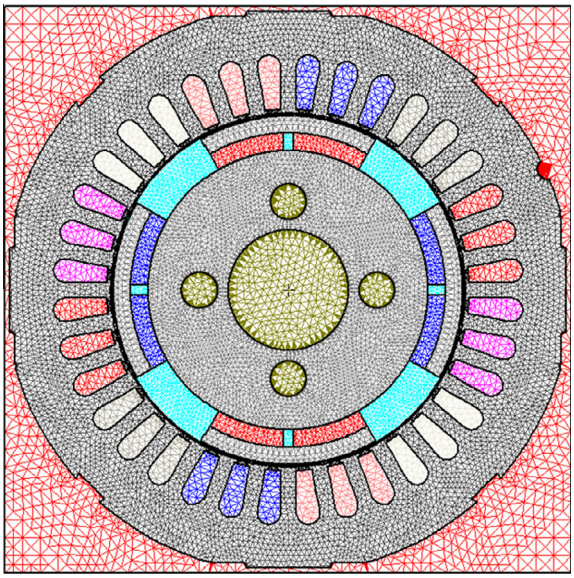

Fig. 5. Finite element mesh layout.

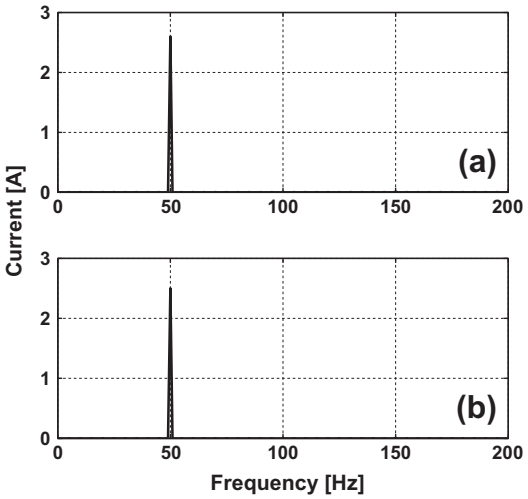

Fig. 6. Phase current frequency spectra, serial winding connection, for (a) $\mu = 0\%$, (b) $\mu = 16.7\%$. Simulation results.

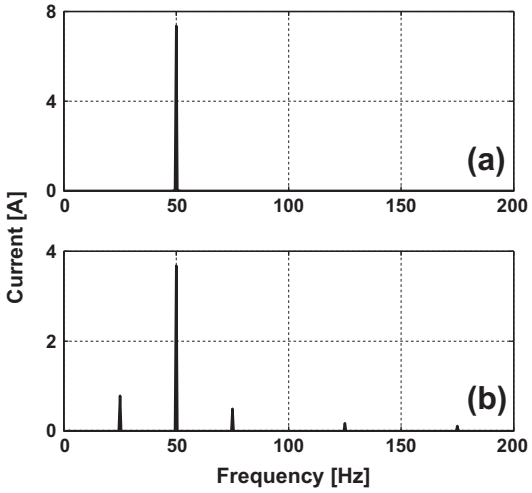

Fig. 7. Current frequency spectra, with $\mu = 16.7\%$ and full load, of phase a (a) and branch $a1$ (b). Simulation results.

The noticeable difference between the magnetic permeability of the steel and the air is responsible for the flux lines contained inside the magnetic core and, for this reason, on the external surface of the stator, a Dirichlet boundary condition was imposed.

A transient analysis was done to obtain the electric dynamics, whereas the mechanical dynamics is neglected by assuming that the machine is operating at constant (rated) speed. Other parameters used on the model are: the maximum error between iterations, the total time of analysis, and the pitch of calculations, so that the waveform reaches its optimum resolution.

Two connection schemes were implemented for the motor windings with the objective of analyzing the effects of faults. A connection in series of the stator windings constitutes the first circuit (Fig. 1). The second circuit is a connection in parallel of them (Fig. 2). A three-phase resistive load was used for both cases.

4. Simulation results

4.1. Serial connection of windings

A connection in series of the stator windings is first considered. Two simulations were carried out: one of them for no fault ($\mu = 0\%$) and other with a partial demagnetization in a pole ($\mu = 16.7\%$). Simulation results of the current spectrum for one of the motor phases are shown in Fig. 6. By analyzing the frequency components for both signals through the FFT, it can be observed that there is a reduction in amplitude of the fundamental components. However, as it was demonstrated analytically, no new components appear in the spectrum due to asymmetrical demagnetization. For the machine operating at rated power, as the induced EMF is reduced, the current results higher than the corresponding rated value. This produces an increase in the winding temperature due to Joule effects.

4.2. Parallel connection of windings

A further stage in this analysis consists in connecting two circuits in parallel as the one shown in Fig. 2. Four cases were analyzed: the first one for no fault ($\mu = 0\%$) and the other three for different levels of demagnetization ($\mu = 4\%$, $\mu = 16.7\%$ and $\mu = 33.3\%$). These levels correspond to demagnetization produced in the laboratory prototype used to obtain the experimental results shown in the next section. For all these cases, the current waveforms corresponding to phase a (i_a) and branch 1 of this phase (i_{a1}) were obtained through simulation.

The spectra of the phase a current for the faulty case are shown in Fig. 7a. As it can be clearly seen, no new components appear. Meanwhile, Fig. 7b presents the analysis of the failure for branch $a1$ current, for the same load conditions. The indicator of fault is given by the magnitude of the components at $\frac{1}{2}f_s$ and $\frac{3}{2}f_s$, which increase as demagnetization increases. The difference between phase and branch currents is due to a circulating current through the two branches. Additionally, components of lower amplitude at frequencies $\frac{5}{2}f_s$ and $\frac{7}{2}f_s$ appear in the spectrum of the branch currents due to demagnetization.

Based on these results, the fault severity factor (21) was evaluated for different demagnetization levels and load conditions, and the obtained results are shown in Fig. 8. As it can be appreciated, the proposed fault severity factor approximates the percentage of pole demagnetization in all the cases, for different load conditions.

For the analyzed case, the reduction of the EMF produced by demagnetization increases the phase currents when the PMSM is

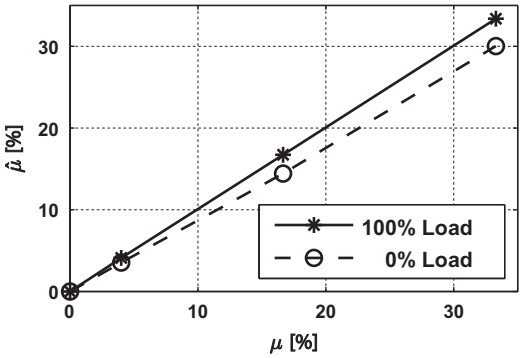

Fig. 8. Fault severity factor $\hat{\mu}$ as a function of the fault severity μ for different load conditions. Simulation results.

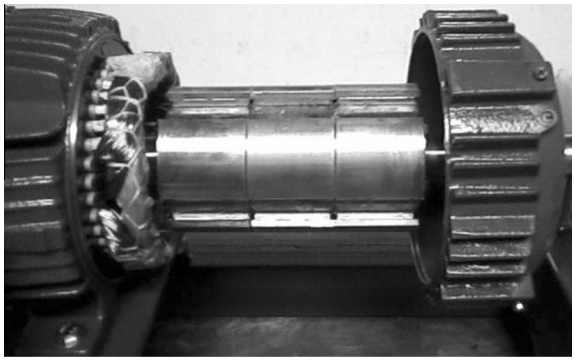

Fig. 9. PMSM prototype used for the experimental results.

operating at rate load. Additionally, for windings connected in parallel the components at $\frac{1}{2}f_s$ and $\frac{3}{2}f_s$ frequencies and their harmonics appear in the branch current spectrum. These effects increase the RMS current in the windings generating additional Joule losses. Such effects are analyzed in detail in the next section.

5. Experimental results

This section presents experimental results from a PMSM prototype whose geometry was previously analyzed through simulation (Fig. 9). The experimental setup is shown in Fig. 10. The PMSM voltages and currents were acquired using a National Instruments USB acquisition board with 12 bits resolution A/D conversion. The PMSM was propelled by an induction motor drive with speed control. The PMSM was loaded with a variable resistive load bank.

In the first experimental test, one phase current and one branch current were measured in the healthy machine. Same measurements were carried out for different load conditions. For this test small sidebands appear on the branch current. Such sidebands

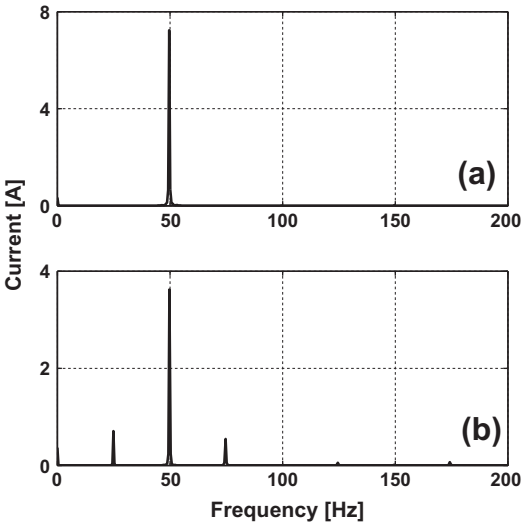

Fig. 11. Current frequency spectra, faulty machine ($\mu = 16.7\%$), with full load and parallel connection, of phase a (a) and branch $a1$ (b). Experimental results.

are produced by differences in magnetization of the magnets, small eccentricities and non-uniform distribution of the air-gap. This case is taken as a reference case, with a fault severity factor below 3%.

Then, a portion of magnet was removed producing a demagnetization of approximately 4% in one pole. Later, one and two of the six magnets that constitute a machine pole were removed, producing a reduction of 16.7% and 33.3% in residual magnetism respectively. Phase and branch currents were measured for this modified machine. Fig. 11 shows the spectra of the phase and branch currents for a demagnetization of 16.7%, and full load conditions.

Fig. 12 presents the fault severity factor $\hat{\mu}$ proposed in (21), as a functions of the fault severity μ for two different load conditions.

The fault severity factor $\hat{\mu}$ as a function of machine load for different demagnetization conditions is shown in Fig. 13. From the same figure, it can be concluded that the proposed severity factor hardly changes with load. For the case without fault, severity factor does not exceed 3%. These values are produced by differences in the magnetization of the magnets, small eccentricities and non-uniform distribution of the air-gap that are inherent of the manufacturing process.

5.1. Derating produced by rotor demagnetization

The asymmetrical rotor demagnetization produces a voltage reduction and an increase of branch currents for the same phase current. These effects produce a reduction in the power available at the generator terminals. To assess these effects, the voltage at the generator terminals as a function of load for different levels of demagnetization is shown in Fig. 14.

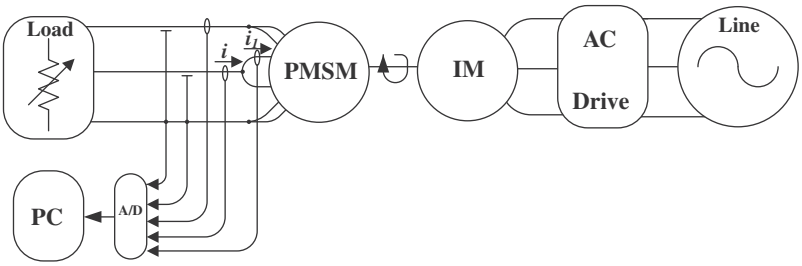

Fig. 10. Experimental setup.

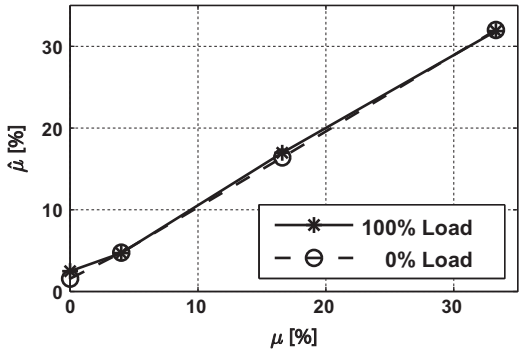

Fig. 12. Fault severity factor $\hat{\mu}$ as a function of the fault severity μ for different load conditions. Experimental results.

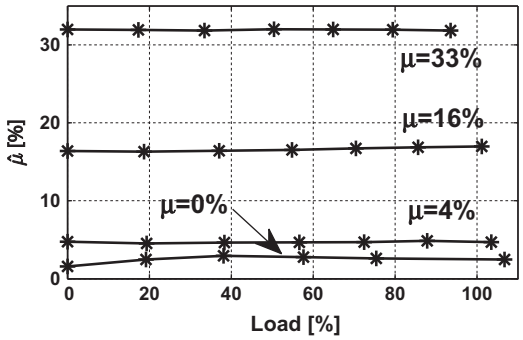

Fig. 13. Fault severity factor as a function of load for different demagnetization conditions. Experimental results.

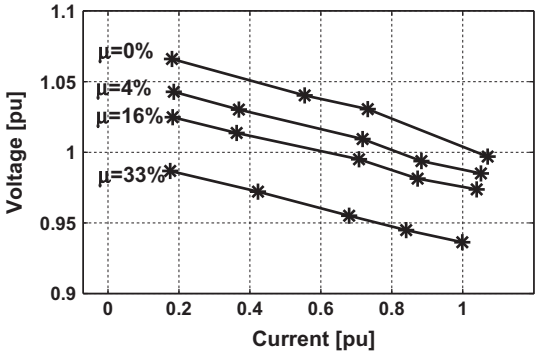

Fig. 14. Voltage as a function of load current for different demagnetization conditions. Experimental results.

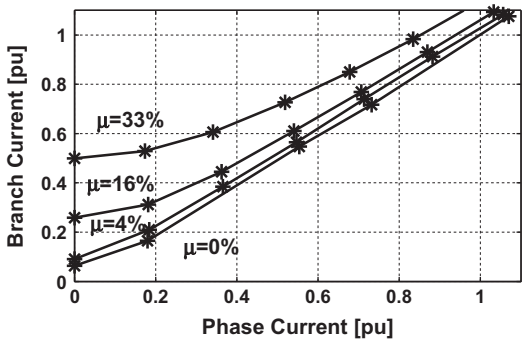

Fig. 15. Branch current vs. phase current for different demagnetization conditions. Experimental results.

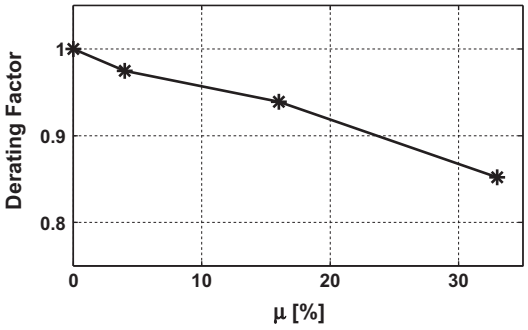

Fig. 16. Derating factor for different asymmetrical demagnetization conditions. Experimental result.

Fig. 15 shows the rms current in a branch as a function of the phase current for different levels of demagnetization.

Because of this effect, the phase current should be reduced depending on magnet demagnetization to ensure that the branch currents do not exceed their rated value. To avoid overheating, a derating factor is defined for the PMSM with asymmetrical demagnetization. Derating factors are commonly used to protect electrical machines from voltage disturbances such as harmonics or unbalance [30,31]. A derating factor for phase currents obtained from the previous results is presented in Fig. 16.

6. Discussion and conclusions

From the analysis presented in this work, it can be concluded that, for a generator with all the windings connected in series, demagnetization on a single magnet produce a reduction of the induced EMF value. If load is resistive type, such reduction appears also in the current. It is not possible to observe frequency components associated to fault, but only a reduction of the total flux linked by the windings.

For the generator with windings connected in parallel, partial demagnetization effects can be observed in the branch currents as new components at $\frac{nf_s}{P}$ (n odd). This is a clear sign of rotor fault in the PMSM. These components only circulate inside the motor windings and do not interfere at all with the phase current. If there is only one magnet with less residual induction, the proposed severity factor that uses the amplitude of the components at $\frac{1}{2}f_s$ and $\frac{3}{2}f_s$ for a PMSM with two pair of poles, is a clear indicator of fault for any load condition.

It is really important to detect and locate incipient rotor faults in PMSMs in order to avoid windings overheating produced by the increase in branch currents, and in consequence maintain the machine properly. With this aim, a derating factor is proposed in this paper, which allows protecting the machine by limiting the maximum phase current.

The strategy proposed in this paper can also be used for the analysis of rotor dynamic eccentricity.

Acknowledgments

This work was supported by the Universidad Nacional de Río Cuarto, by the Universidad Nacional del Centro de la Provincia de Buenos Aires, by the FONCyT-ANPCyT and by the Consejo Nacional de Investigaciones Científicas y Técnicas (CONICET).

References

[1] Ki-Chan K, Seung-Bin L, Ki-Bong J, Sung-Gu L, Ju L, Yeoung- Gyu S, et al. Analysis on the direct-driven high power permanent magnet generator for

wind turbine. In: Proceedings of the eighth international conference on electrical machines and systems (ICEMS 2005), vol. 1; 2005. p. 243–47.
[2] Wang F, Bai J, Hou Q, Pan J. Design features of low speed permanent magnet generator direct driven by wind turbine. In: Proceedings of the eighth international conference on electrical machines and systems (ICEMS 2005), vol. 2; 2005. p. 1017–20.
[3] Amirat Y, Benbouzid MEH, Bensaker B, Wamkeue R. Condition monitoring and fault diagnosis in wind energy conversion systems: a review. In: IEEE international electric machines & drives conference (IEMDC '07), vol. 2; 2007. p. 1434–39.
[4] Rajagopalan S, Aller JM, Restrepo JA, Habetler TG, Harley RG. Detection of rotor faults in brushless DC motors operating under nonstationary conditions. IEEE Trans Ind Appl 2006;42(6):1464–77.
[5] Ebrahimi B-M, Faiz J, Roshtkhari MJ. Static-, dynamic-, and mixed-eccentricity fault diagnoses in permanent-magnet synchronous motors. IEEE Trans Ind Electron 2009;56(11):4727–39.
[6] Yao Duan, Toliyat H. A review of condition monitoring and fault diagnosis for permanent magnet machines. In: Power and energy society general meeting, 2012 IEEE, 22–26 July 2012. p. 1–4
[7] Toliyat HA, Al-Nuaim NA. Simulation and detection of dynamic air-gap eccentricity in salient-pole synchronous machines. IEEE Trans Ind Appl 1999;35(1):86–93.
[8] Nandi S, Toliyat HA, Xiaodong Li. Condition monitoring and fault diagnosis of electrical motors-a review. IEEE Trans Energy Convers 2005;20(4):719–29.
[9] Le Roux W, Harley R, Habetler T. Rotor fault analysis of a permanent magnet synchronous machine. In: International conference on electrical machines (ICEM'02), Brugge, Belgium; 2002.
[10] Rajagopalan S, le Roux W, Habetler TG, Harley RG. Diagnosis of potential rotor faults in brushless dc machines. In: Second international conference on power electronics, machines and drives (PEMD 2004), vol. 2; 2004. p. 668–73 (Conf. Publ. No. 498).
[11] Rajagopalan S, Roux W, Habetler TG, Harley RG. Dynamic eccentricity and demagnetized rotor magnet detection in trapezoidal flux (brushless dc) motors operating under different load conditions. IEEE Trans Power Electron 2007;22(5):2061–9.
[12] Bellini A, Filippetti F, Tassoni C, Capolino GA. Advances in diagnostic techniques for induction machines. IEEE Trans Ind Electron 2008;55(12):4109–26.
[13] Aydin I, Karakose M, Akin E. A new method for early fault detection and diagnosis of broken rotor bars. Energy Convers Manage 2011;52(4):1790–9.
[14] Acosta GG, Verucchi C, Gelso E. A current monitoring system for diagnosing electrical failures in induction motors. Mech Syst Signal Process 2006;20(4):953–65.
[15] Faiz J, Ebrahimi BM, Toliyat HA, Abu-Elhaija WS. Mixed-fault diagnosis in induction motors considering varying load and broken bars location. Energy Convers Manage 2010;51(7):1432–41.
[16] Bossio GR, De Angelo CH, Bossio JM, Pezzani CM, Garcia GO. Separating broken rotor bars and load oscillations on IM fault diagnosis through the instantaneous active and reactive currents. IEEE Trans Ind Electron 2009;56(11):4571–80.
[17] Ebrahimi BM, Etemadrezaei M, Faiz J. Dynamic eccentricity fault diagnosis in round rotor synchronous motors. Energy Convers Manage 2011;52(5):2092–7.
[18] Royo J, Segui R, Pardina A, Nevot S, Arcega FJ. Machine current signature analysis as a way for fault detection in permanent magnet motors in elevators. In: The 18th international conference on electrical machines (ICEM 2008); 2008. p. 1–6.
[19] Vaseghi B, Takorabet N, Nahid-Mobarakeh B, Meibody-Tabar F. Modelling and study of PM machines with inter-turn fault dynamic model–FEM model. Electric Power Syst Res 2011;81(8):1715–22.
[20] Le Roux W, Harley RG, Habetler TG. Detecting faults in rotors of PM drives. IEEE Ind Appl Mag 2008;14(2):23–31.
[21] Urresty J, Riba JR, Delgado M, Romeral L. Detection of demagnetization faults in surface-mounted permanent magnet synchronous motors by means of the zero-sequence voltage component. IEEE Trans Energy Convers 2012;27:42–51.
[22] le Roux W, Harley RG, Habetler TG. Detecting rotor faults in low power permanent magnet synchronous machines. IEEE Trans Power Electron 2007;22(1):322–8.
[23] Le Roux W, Harley RG, Habetler TG. Detecting rotor faults in permanent magnet synchronous machines. In: The 4th IEEE international symposium on diagnostics for electric machines, power electronics and drives (SDEMPED 2003); 2003. p. 198–203.
[24] Casadei D, Filippetti F, Rossi C, Stefani A. Magnets faults characterization for permanent magnet synchronous motors. In: The 7th IEEE international symposium on diagnostics for electric machines, power electronics and drives (SDEMPED'09), Cargese, France; 2009. p. 6.
[25] Min D, Keyhani A, Sebastian T. Fault analysis of a PM brushless DC motor using finite element method. IEEE Trans Energy Convers 2005;20(1):1–6.
[26] Hajiaghajani M, Lei H, Madani SM, Toliyat HA. A method for detection of eccentricity in permanent magnet machines. In: Conference record of the industry applications conference, 38th IAS annual meeting, vol. 3; 2003. p. 1833–38.
[27] Chen HS, Tsai MC. Effect of rotor eccentricity on electric parameters in a PM brushless motor with parallel winding connections. J Appl Phys 2009;105(7):07F121–>.
[28] Ruschetti C, Bossio G, De Angelo C, Verucchi C. Effects of partial rotor demagnetization on permanent magnet synchronous machines. IEEE Int Conf Ind Tech (ICIT) 2010:1233–8.
[29] Batistela NJ. Caracterização e Modelagem Eletromagnética de Lâminas de Aço ao Silício. Ph.D. thesis. Universidade Federal de Santa Catarina; Brazil: 2001.
[30] Donolo PD, Bossio GR, De Angelo C. Analysis of voltage unbalance effects on induction motors with open and closed slot. Energy Convers Manage 2011;52(5):2024–30.
[31] Gnacinski P. Derating of an induction machine under voltage unbalance combined with over or undervoltages. Energy Convers Manage 2009;50(4):1101–7.